Indoor Drone Propeller Speed Estimation Using Wi-Fi Channel State Information

Yuta Takao*, Viktor Erdélyi*†, Kazuya Ohara‡, Yasue Kishino§, Anh-Van Ho¶, Akira Uchiyama*†
*The University of Osaka, Suita, Osaka 565–0871, Japan
Email: {y-takao, viktor, uchiyama}@ist.osaka-u.ac.jp
†RIKEN Center for Computational Science, Kobe, Hyogo 650–0047, Japan
‡NTT Access Network Service Systems Laboratories, Yokosuka, Kanagawa 239–0847, Japan
Email: kazuya.ohara@ntt.com
§NTT Communication Science Laboratories, Seika, Kyoto 619–0237, Japan
Email: yasue.kishino@ntt.com
¶Japan Advanced Institute of Science and Technology, Nomi, Ishikawa 923–1292, Japan
Email: van-ho@jaist.ac.jp

***Abstract*—Accurate measurement of propeller rotation speed is essential for stable drone control. While various sensors have been employed for this purpose, their cost, size, and additional weight pose challenges, particularly for small indoor drones. This paper presents a method for estimating propeller rotational speed using Wi-Fi Channel State Information (CSI), which captures fine-grained wireless signal fluctuations and is obtainable on many commercial Wi-Fi devices. The proposed approach applies resampling and short-time Fourier transform (STFT) to the amplitude component of CSI to estimate propeller rotational speed. In this study, experiments were conducted using both fixed propellers and a hovering drone in indoor environments. The results revealed that antenna placement and polarization alignment significantly affect the accuracy of rotation speed estimation. With a tilted antenna configuration, the estimation error rate remained below 3.16% in all STFT windows (each 0.5-second estimation interval). Furthermore, even with a horizontally placed antenna, selecting dominant subcarriers through signal processing reduced the estimation error rate to below 4% in over 95% of STFT windows. In addition, by evaluating three distances (2 m, 4 m, and 8 m) and varying the antenna elevation from 0° to 90°, we identified optimal orientations that reduced RMSE to as low as 23.60 RPM, achieving a mean error of only 1.24 % at 8 m. These findings demonstrate the feasibility of non-contact propeller rotational speed estimation using Wi-Fi CSI and suggest its potential for real-time control applications.**

***Index Terms*—Wi-Fi CSI, Propeller Speed Estimation, Indoor Drones, Wi-Fi Sensing**

I. Introduction

The demand for drones is rapidly expanding, with applications not only in outdoor scenarios such as logistics, surveillance, infrastructure inspection, and agriculture, but also in indoor environments including warehouse inventory management, item delivery, and entertainment [1].

As drones become increasingly integrated into everyday operations, accurately estimating propeller rotational speed (revolutions per minute, RPM) is essential for maintaining flight stability and enabling post-collision recovery. We refer to this as RPM estimation throughout this paper. RPM estimation also enables drone detection and payload assessment [2].

Traditional approaches rely on mounting encoder sensors on the motor shaft [3], which, while precise, add cost and weight—factors that are particularly problematic for small indoor drones. Alternatives such as camera-based [2] or motor-current-based methods [4] have been explored. However, camera systems require high frame rates and controlled lighting, while current-based methods offer limited accuracy.

Radio-frequency (RF)-based techniques provide a promising alternative: they operate independently of lighting conditions and do not require onboard sensors. For instance, Abdelnasser et al. [5] proposed using 5GHz RF and 77GHz mmWave radar. While mmWave radar demonstrated high accuracy at longer distances, its high implementation cost limits practical use. On the other hand, 5GHz solutions are more accessible but suffer from short range and environmental noise sensitivity.

To address these challenges, we explore a non-contact method that estimates propeller RPM using Wi-Fi Channel State Information (CSI). CSI captures fine-grained variations in wireless signals between a transmitter and a receiver, which reflect environmental dynamics such as propeller motion. Since most drones are already equipped with Wi-Fi modules, our method requires no additional hardware. The proposed approach applies resampling and short-time Fourier transform (STFT) to the amplitude component of CSI to estimate RPM. Furthermore, the proposed approach introduces dominant subcarrier selection to improve RPM estimation accuracy. This selection increases the effective signal-to-noise ratio (SNR), enhancing the reliability of peak detection. By retaining only those subcarriers whose amplitude exhibits strong and stable signatures from the propeller blades, the periodic peak in the frequency domain becomes sharper, leading to lower variance and higher robustness against interference and multipath fading.

We experimentally evaluate a non-contact method for estimating the propeller rotation speed of drones in indoor environments using Wi-Fi CSI. We first conduct a basic performance evaluation using a fixed propeller, followed by experiments with a hovering drone to analyze the factors affecting

979-8-3503-9281-4/25/$31.00 ©2025 IEEE

estimation accuracy. The results show that antenna placement and polarization alignment significantly affect the estimation accuracy. Nevertheless, the proposed method achieves the 4% RPM error in over 95% of STFT windows with the help of the dominant subcarrier selection. In addition, by evaluating three distances (2 m, 4 m, and 8 m) and varying the antenna elevation from 0° to 90°, we identified optimal orientations that reduced RMSE to as low as 23.60 RPM, achieving a mean error of only 1.24 % at 8 m, performance comparable to 77 GHz millimeter-wave radar techniques [5].

II. Related Work

A. Contact-Based Estimation

Contact-based approaches require physically attaching sensors to the rotating shaft of the propeller. The most common solution is to use encoders [3]. Encoders are available in optical, magnetic, and capacitive types. *Optical encoders* detect light pulses passing through slits on a rotating disk. These signals are converted into electrical pulses and can measure rotation speed with high precision. However, they are sensitive to contaminants such as oil, dust, or moisture. *Magnetic encoders* detect changes in magnetic fields caused by rotating magnets attached to the shaft. They are robust against environmental interference but may be affected by electromagnetic noise and have limited operating temperature ranges. *Capacitive encoders* use PCB-based rotation patterns and detect changes in electric fields. They are resistant to contamination and temperature variations and can achieve higher resolution compared to magnetic types.

Another approach involves detecting electrostatic signals generated by friction [6], [7]. This approach can be effective, but it is sensitive to electromagnetic interference and environmental factors such as humidity.

The above methods require sensor attachment, which is undesirable for small indoor drones due to added weight and complexity. In contrast, our proposed Wi-Fi CSI–based approach requires no physical sensors on the propeller shaft, avoiding additional weight and system complexity.

B. Non-Contact-Based Estimation

Non-contact-based approaches do not require sensors to be attached to the drone. These methods are preferable in lightweight scenarios such as small indoor drones.

Vision-based methods use cameras to estimate rotation by analyzing captured images frame by frame [8], [9]. However, they are constrained by frame rate limitations, lighting conditions, and cost if high-speed cameras are required.

RF-based methods have gained attention due to their robustness to external conditions. Abdelnasser et al. [5] demonstrated Doppler-based analysis using 5 GHz and 77 GHz radar. The 5 GHz system achieved high accuracy (e.g., 16 000 RPM with 0.63% error), but was limited to short ranges (about 1 m). In contrast, 77 GHz millimeter-wave radar supported longer distances (up to 8 m) with acceptable error rates (1.5 %) but suffered from high deployment costs.By comparison, our method can leverage existing Wi-Fi modules onboard the drone, enabling non-contact propeller speed estimation over several meters without extra sensors or expensive hardware.

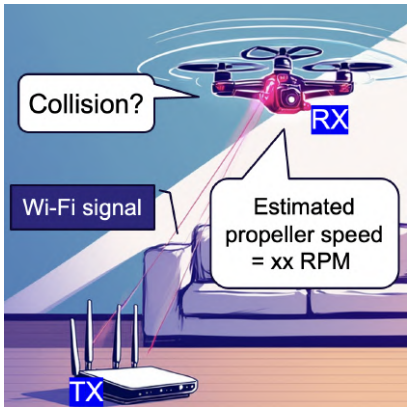

Fig. 1. Assumed indoor setup using a Wi-Fi access point and a drone

III. Proposed Method

A. Background on Wi-Fi CSI

Wi-Fi uses Orthogonal Frequency Division Multiplexing (OFDM) to transmit data via multiple subcarriers. Channel State Information (CSI) captures amplitude and phase alterations of signals during transmission, represented as a 3D matrix $H[k, p, t]$, where k is the subcarrier index, p is the antenna pair (path) index, and t is the time index. Each entry is a complex number:

$$H[k, p, t] = A[k, p, t] \cdot e^{j\phi[k,p,t]},$$

where A and ϕ denote amplitude and phase, respectively.

B. Overview

Our method assumes an indoor Wi-Fi access point acts as the transmitter, while a drone-mounted Wi-Fi module serves as the receiver, as shown in Fig. 1. Our system continuously transmits and captures CSI packets containing complex amplitude and phase data. However, since the phase is often noisy, in this paper, we focus solely on amplitude to validate feasibility.

The amplitude of the CSI varies periodically depending on the angle of the propeller. Fig. 2 shows the average amplitude of a single subcarrier measured while the propeller was held stationary, with its orientation incrementally changed by 30 degrees. The figure shows that the amplitude changes depending on the propeller's angle. When the propeller rotates, such angle-dependent variations appear periodically over time. Therefore, by performing frequency analysis on the amplitude time series, the rotational speed can be estimated.

An overview of our proposed estimation process is shown in Fig. 3. After collecting CSI amplitude data of size $k \times p \times t$ (k: number of subcarriers, p: number of antenna pairs, defined as $N_{\mathrm{Tx}} \times N_{\mathrm{Rx}}$; t: number of time samples), preprocessing and Fourier transform are applied to each subcarrier–antenna pair. In the flow diagram (Fig. 3), the STFT time windows are indicated as t_x to distinguish them from the raw time indices t. The resulting frequency spectra are then averaged, and the

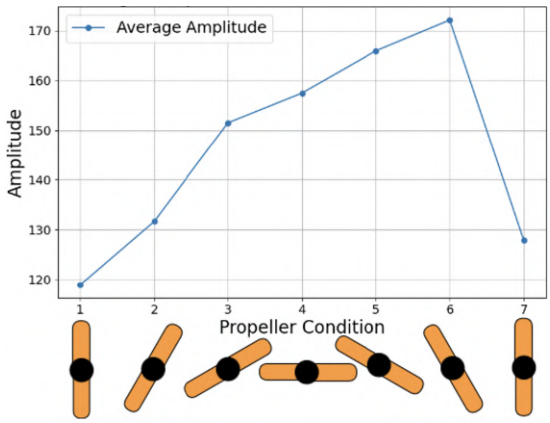

Fig. 2. Average amplitude of a single subcarrier at different propeller angles

rotation speed is estimated by detecting peaks in the spectrum. Additionally, to enhance robustness by focusing on subcarriers that contain more relevant frequency components, a subcarrier selection step can also be introduced.

C. Preprocessing

CSI from Wi-Fi transmissions has non-uniform sampling intervals, which STFT cannot handle directly. We resampled the data at 1 kHz (matching the average CSI sampling rate) using linear interpolation to ensure uniform intervals, avoiding noise emphasis and aliasing. A Hanning window was applied during STFT to minimize spectral leakage while preserving frequency resolution, suitable for periodic signals like propeller rotation and real-time processing.

D. Frequency Spectrum via Fourier Transform

We apply STFT to the resampled time-series of CSI amplitude to obtain frequency-domain representations. The STFT uses a window size of 500 samples with 50 % overlap, resulting in a frequency resolution of 2 Hz. This corresponds to a resolution of approximately 60 RPM, which is sufficient for estimating common drone propeller speeds ranging from 4000 RPM to 10 000 RPM. We applied no additional zero-padding beyond the default behavior of Python's scipy.signal.spectrogram function, which pads only as required by the specified window size and overlap parameters.

STFT is applied to all k subcarriers, and the resulting spectrograms are averaged to reduce noise. For each STFT window, the dominant peak is detected to estimate the propeller speed at 0.5 s intervals. Peaks below 30 Hz are excluded based on empirical observation of minimum propeller rotation.

E. Subcarrier Selection Based on Propeller Frequency Prominence

To emphasize signal components caused by propeller rotation and improve estimation accuracy, we introduce a subcarrier selection method based on *propeller band dominance*. Since Wi-Fi OFDM subcarriers and antenna pairs exhibit different frequency-selective fading characteristics, simply averaging across all subcarriers incorporates noise and unrelated motion, reducing reliability. Thus, we employ subcarrier selection based on a spectral energy ratio metric, inspired by CSI-based respiration monitoring [10]. We define the spectral power of subcarrier k and antenna pair p at time t and frequency f, obtained via STFT, as $S_{k,p}(f,t)$. Then, we define the propeller band dominance ratio $R_{k,p,t}$ as:

$$R_{k,p,t} = \frac{\sum_{f \geq 30} S_{k,p}(f,t)}{\sum_{f \geq 0} S_{k,p}(f,t)}. \tag{1}$$

This ratio quantifies energy concentration in the target frequency band above 30 Hz compared to the total spectral power, essentially evaluating each subcarrier's propeller-induced signal content. This frequency corresponds to the minimum observed propeller speed of approximately 1000 RPM. Next, we compute the maximum dominance ratio at time t, denoted as $R_{\max,t}$, and select subcarriers satisfying:

$$R_{k,p,t} \geq \alpha \cdot R_{\max,t}, \tag{2}$$

where α is a user-defined selection threshold (e.g., 0.99, 0.95). This enables flexible selection of subcarriers whose dominance is sufficiently high compared to the most informative one. Notably, when $\alpha = 1$, only the most dominant subcarrier is selected, whereas $\alpha = 0$ corresponds to using all subcarriers.

The selected subcarrier spectra are averaged for peak detection to estimate rotational speed, enhancing accuracy by suppressing irrelevant components. The number of selected subcarriers varies dynamically over time – selecting few subcarriers when only these exhibit strong propeller components, or many when multiple subcarriers carry meaningful signals. Fixed-number selection would discard useful subcarriers and miss the accuracy improvements.

F. RPM Estimation

The rotation speed (RPM) is calculated from the dominant peak frequency f_{peak} in the frequency domain using the following equation:

$$\omega_{\text{RPM}} = \frac{60 \cdot f_{\text{peak}}}{n} \tag{3}$$

where n is the number of propeller blades. The factor 60 converts Hz to RPM. Since each blade contributes to one frequency cycle per revolution, the estimated frequency is proportional to the blade count. Given a sampling rate of 1000 Hz, the Nyquist frequency is 500 Hz, allowing up to 15 000 RPM to be detected when $n = 2$. This is sufficient for most commercial drones.

IV. Evaluation

This section presents experiments conducted to validate the proposed method. We evaluate performance starting with a fixed propeller setup, then advance to experiments using an actual hovering drone. To enhance signal reflection, the propeller surface was coated with aluminum. The analysis procedures, results, and discussions for each experiment are described in order.

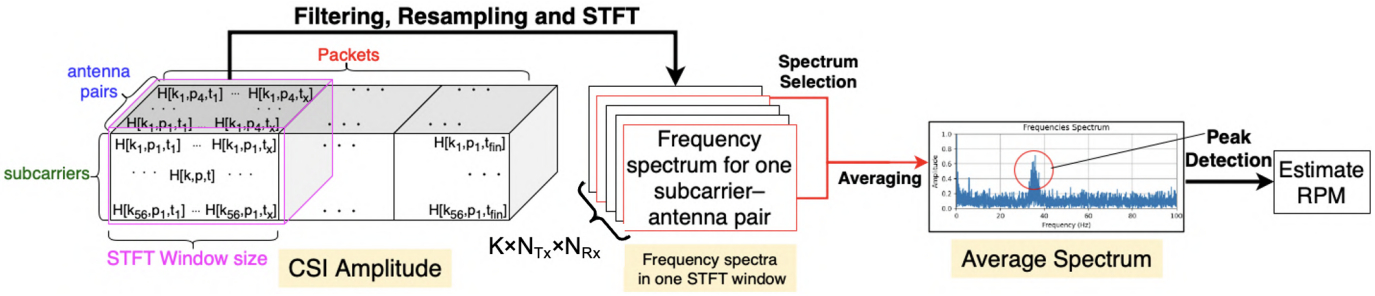

Fig. 3. Flow of proposed RPM estimation method

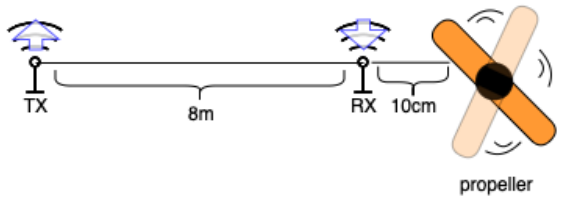

Fig. 4. Setup for the fixed propeller experiment

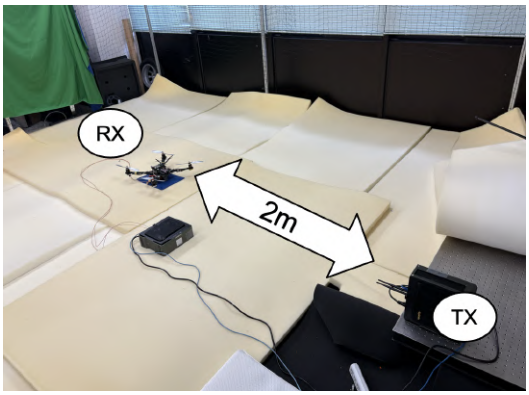

Fig. 5. Experimental setup using an actual drone

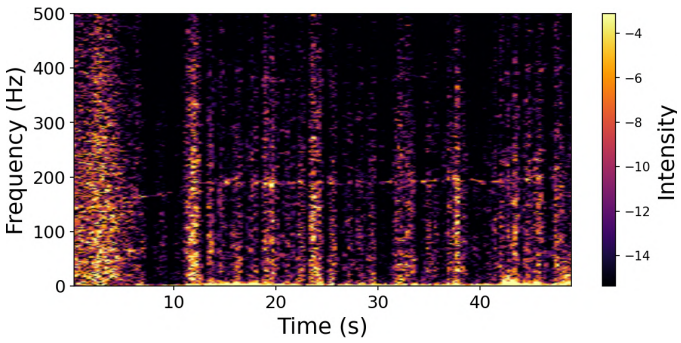

Fig. 6. Spectrogram in real drone environment

The experiments were conducted in an indoor laboratory environment with external Wi-Fi interference. Both the transmitter and receiver were implemented using mini PCs equipped with Intel AX210 Wi-Fi modules. On the transmitter side, packets were sent at $1\,\mathrm{ms}$ intervals using injection mode, while the receiver recorded CSI using PicoScenes [11].

Note that in all experiments except Section IV-E, the frequency spectra were computed by averaging all subcarriers (i.e., without selection, equivalent to $\alpha = 0$). Section IV-E introduces adaptive subcarrier filtering to improve robustness by excluding noisy subcarriers. In all experiments, ground truth was obtained using a capacitive rotary encoder (AMT10E series [12]) interfaced to a microcontroller, acquiring measurements at 100 Hz.

A. Preliminary Evaluation with Fixed Propeller

First, we evaluated our system in a simple configuration using a fixed propeller. As shown in Fig. 4, the transmitter (Tx) and receiver (Rx) were placed $8.1\,\mathrm{m}$ and $10\,\mathrm{cm}$ apart with the propeller, respectively. The propeller was oriented vertically relative to the ground. CSI was recorded for 30 seconds at constant rotational speed, then resampled to $1000\,\mathrm{Hz}$ and processed using FFT to extract the dominant frequency peak. The estimation error remained within $1.1\,\%$ even when the Tx-Rx distance was extended to $8\,\mathrm{m}$, demonstrating the effectiveness of the proposed method.

B. Evaluation with Hovering Drone

For this experiment, as shown in Fig. 5, we used a custom-built quadrotor drone, assembled from commercially available components. The drone was kept hovering at a height of $1\,\mathrm{m}$ while CSI data was collected.

STFT was applied to the recorded data, and the resulting spectrogram is presented in Fig. 6. The estimated rotational speeds, derived from the peak frequency in each STFT window, are compared with ground truth values from an attached encoder in Fig. 7.

As shown in Fig. 6, the peak around $200\,\mathrm{Hz}$ corresponding to the rotation frequency is significantly less prominent, and Fig. 7 indicates that the estimated RPM fluctuates considerably. Possible reasons for this degradation in estimation accuracy include signal attenuation due to the length of the SMA (Sub-Miniature version A) cables, interference from multiple propellers, and vibrations of the drone body. Additionally, unlike the basic evaluation experiments where the propeller and antennas were oriented vertically relative to the ground, the setup employed a horizontal alignment, which may have also affected the results. To verify these hypotheses, the next

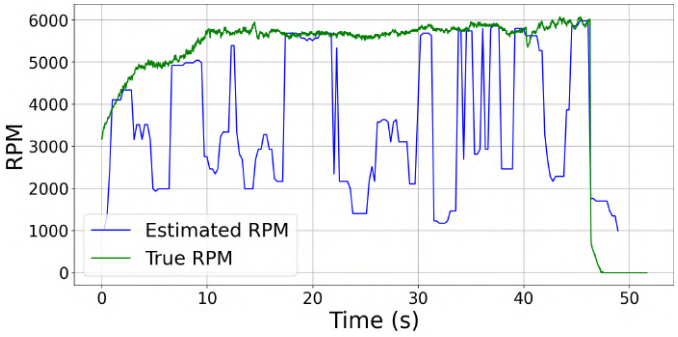

Fig. 7. Comparison between estimated and ground truth encoder RPM

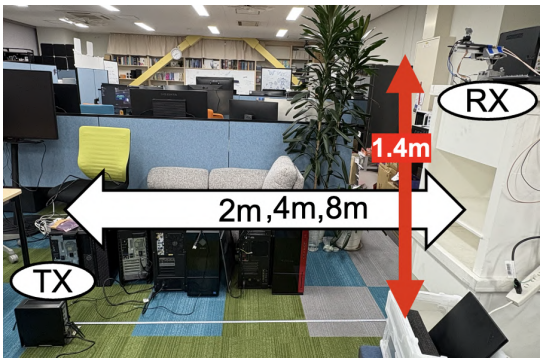

Fig. 8. Setup of simulated hovering experiment using a fixed propeller

section presents comparative experiments with varied Tx-Rx distances.

C. Simulated Hovering Experiment

We conducted experiment simulating hovering using a fixed propeller at a distance of $2\,\mathrm{m}$ with the height of $1.4\,\mathrm{m}$ as shown in Fig. 8. In this experiment, we compared the rotational speed estimation accuracy between a horizontally aligned transmitting antenna and one tilted to direct its beam toward the propeller. The estimated RPMs and ground truth values obtained from the encoder were plotted at $0.5\,\mathrm{s}$ intervals, as shown in Figs. 9(a) and 9(b), respectively.

As a result, the Root Mean Square Error (RMSE) was $937.28\,\mathrm{RPM}$ when the antenna was placed horizontally, whereas it significantly decreased to $26.15\,\mathrm{RPM}$ when the antenna was tilted. This clearly demonstrates the effectiveness of antenna angle adjustment in improving estimation accuracy.

D. Estimation Accuracy by Distance and Angle

To assess how antenna elevation angle impacts estimation accuracy at various distances, we fixed the drone–antenna distance at $2\,\mathrm{m}$, $4\,\mathrm{m}$, and $8\,\mathrm{m}$ (see Fig. 8) and varied the transmitting antenna's angle relative to the ground from $0°$ to $90°$. The resulting RMSE at each angle and distance is plotted in Fig. 10. The results indicate that, for each distance, there exists an optimal antenna angle that minimizes estimation error. In particular, at $8\,\mathrm{m}$ range, $60°$ elevation achieved the mean error of only $1.24\,\%$, comparable to 77 GHz millimeter-wave radar techniques [5]. This result highlights that our method can achieve drone propeller speed estimation with high accuracy, by adjusting the antenna angle appropriately. We note that a beamforming technique can be applied to optimize the beam direction instead of changing the antenna angle.

E. Improving Estimation via Subcarrier Selection

Finally, to improve estimation accuracy without adjusting the antenna angle, we evaluated the effectiveness of the subcarrier selection described in Section III-E. Specifically, we examined the impact of including subcarriers whose power ratio was within $79\,\%$ ($\alpha = 0.79$) to $99\,\%$ ($\alpha = 0.99$) relative to the most dominant subcarrier in each time window. For each threshold, RMSE between the estimated and ground truth rotation speed was calculated. The results are shown in Fig. 11. The number of selected subcarriers for each threshold is also shown to analyze the relationship between estimation accuracy and the number of subcarriers used.

The result indicates that while reducing the number of subcarriers generally improves estimation accuracy, using only a single subcarrier leads to a degradation in performance, suggesting that there exists an optimal number of subcarriers to include for robust estimation.

Among these thresholds, the lowest RMSE was obtained when selecting the subcarriers with the power ratio no less than $99\,\%$ of the most dominat subcarrier. Fig. 9(c) shows the comparison between the estimated and ground truth rotation speed under this setting. With the subcarrier selection, the RMSE was reduced to $260.67\,\mathrm{RPM}$, compared to $937.28\,\mathrm{RPM}$ without the subcarrier selection.

Furthermore, Fig. 12 shows the cumulative distribution functions (CDFs) of the estimation error rate for each STFT window, based on the results in Figs. 9(a), 9(b), and 9(c). As shown in Fig. 12, the tilted antenna configuration achieved an estimation error rate below $3.16\,\%$ in all STFT windows. Additionally, when subcarrier selection was applied under the parallel antenna setup, more than $95\,\%$ of the STFT windows achieved an estimation error rate below $4\,\%$.

These results demonstrate that selecting multiple subcarriers that contain strong frequency components related to the rotation speed can significantly improve estimation accuracy, even without adjusting the antenna angle.

V. Conclusion

In this paper, we proposed a Wi-Fi CSI–based method for estimating the propeller speed of indoor drones. The approach applies STFT to the CSI-amplitude sequence and incorporates subcarrier selection to improve accuracy. Experiments show that the method estimates propeller rotational speed with less than $4\,\%$ error in $95\,\%$ of the STFT windows. Furthermore, by evaluating three different ranges ($2\,\mathrm{m}$, $4\,\mathrm{m}$, and $8\,\mathrm{m}$) and varying the antenna elevation from $0°$ to $90°$, we identified an optimal angle for each distance. In particular, at an $8\,\mathrm{m}$ range a $60°$ elevation achieved a mean error rate of only $1.24\,\%$, comparable to 77 GHz millimeter-wave radar methods [5]. These results highlight that both physical optimization of antenna placement and signal-processing-driven subcarrier

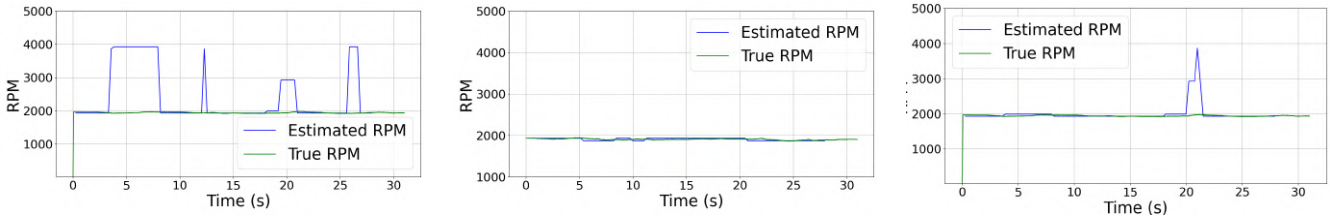

(a) Horizontal antenna (b) Tilted antenna (c) Horizontal antenna and subcarrier selection

Fig. 9. Comparison between estimated and ground truth RPM under different conditions

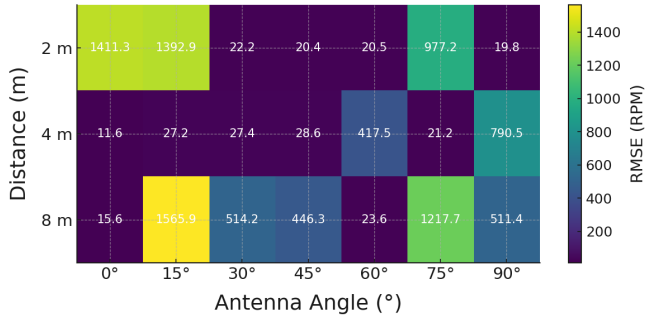

Fig. 10. Heatmap of RMSE versus antenna elevation angle and drone-antenna distance (2 m, 4 m, 8 m).

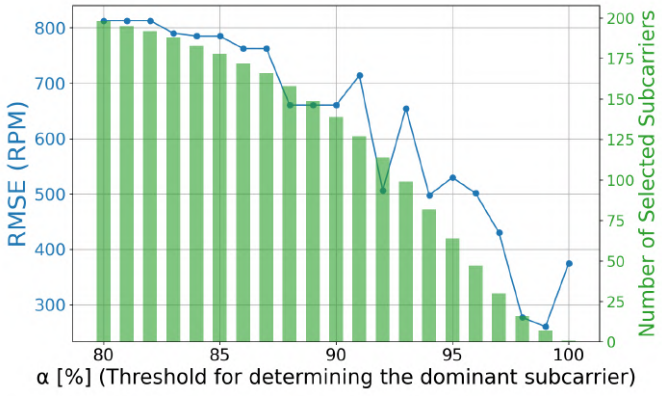

Fig. 11. RMSE transition for each allowed subcarrier ratio

selection are essential for robust, non-contact RPM estimation using CSI. Future work will extend the method to dynamic-flight scenarios and investigate its use for real-time control.

Acknowledgment

This work was partially supported by JST AIP Acceleration Research JPMJFR222T, Japan and the Grant-in-Aid for Scientific Research (B) (Grant number 23K24839) from JSPS. The authors would like to thank Assistant Professor Nguyen Huu Nhan, Mr. Pham Ngoc Quang, and Mr. Hung Tien Pham of the Japan Advanced Institute of Science and Technology for providing the experimental environment and extensive support. The work utilized ChatGPT (OpenAI) to support the refinement of English expression and manuscript organization, and Chroma (Lodestone Rock) to generate Fig. 1.

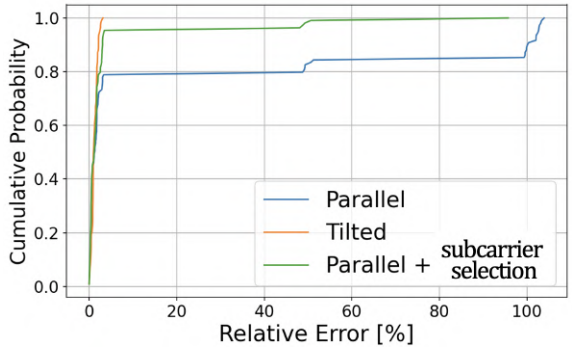

Fig. 12. CDF of absolute estimation error under different settings

References

[1] A. Sen, "Efficient charging and power management system for drone fleets: Revolutionizing aerial operations," *Innovative Research Thoughts*, vol. 9, no. 5, pp. 21–32, 2023.

[2] F. B. D. Dizeu *et al.*, "Extracting unambiguous drone signature using high-speed camera," *IEEE Access*, vol. 10, pp. 45 317–45 336, 2022.

[3] F. Briz, J. Cancelas, and A. Diez, "Speed measurement using rotary encoders for high performance ac drives," in *Proceedings of IECON'94 - 20th Annual Conference of IEEE Industrial Electronics*, vol. 1, 1994, pp. 538–542 vol.1.

[4] K. N. Mogensen, "Motor-control considerations for electronic speed control in drones," Texas Instruments, Tech. Rep., 2016. [Online]. Available: https://www.ti.com/lit/an/slyt692/slyt692.pdf?ts=1739339060585

[5] H. Abdelnasser *et al.*, "Drone propeller speed measurement: Case study using 5ghz rf and mmwave radar," in *2024 IEEE 99th Vehicular Technology Conference (VTC2024-Spring)*. IEEE, 2024, pp. 1–6.

[6] L. Li *et al.*, "Digital approach to rotational speed measurement using an electrostatic sensor," *Sensors*, vol. 19, no. 11, p. 2540, 2019.

[7] L. Wang *et al.*, "Rotational speed measurement through electrostatic sensing and correlation signal processing," *IEEE Transactions on Instrumentation and Measurement*, vol. 63, no. 5, pp. 1190–1199, 2013.

[8] Y. Wang *et al.*, "Rotational speed measurement through digital imaging and image processing," in *2017 IEEE International Instrumentation and Measurement Technology Conference (I2MTC)*, Turin, Italy, 2017, pp. 1–6.

[9] T. Wang *et al.*, "Rotational speed measurement through image similarity evaluation and spectral analysis," *IEEE Access*, vol. 6, pp. 46 718–46 730, 2018.

[10] Y. Zeng *et al.*, "Multisense: Enabling multi-person respiration sensing with commodity wifi," *Proc. ACM Interact. Mob. Wearable Ubiquitous Technol.*, vol. 4, no. 3, Sep. 2020.

[11] Z. Jiang *et al.*, "Eliminating the Barriers: Demystifying Wi-Fi Baseband Design and Introducing the PicoScenes Wi-Fi Sensing Platform," *IEEE IoT Journal*, vol. 9, no. 6, pp. 4476–4496, 2022.

[12] CUI Devices, "AMT10 Series Modular Encoders," 2023, accessed: 2025-02-04. [Online]. Available: https://www.cuidevices.com/product/resource/amt10.pdf